

# Axial current as the origin of quantum intrinsic orbital angular momentum

Orkash Amat <sup>1,\*</sup>, Nurimangul Nurmamat <sup>1</sup>, Yong-Feng Huang <sup>1,2,†</sup>, Cheng-Ming Li <sup>3</sup>, Jin-Jun Geng <sup>4</sup>, Chen-Ran Hu <sup>1</sup>, Ze-Cheng Zou <sup>1</sup>, Xiao-Fei Dong <sup>1</sup>, Chen Deng <sup>1</sup>, Fan Xu <sup>5</sup>, Xiao-li Zhang <sup>6</sup>, and Chen Du <sup>1</sup>

<sup>1</sup>*School of Astronomy and Space Science, Nanjing University, Nanjing 210023, China*

<sup>2</sup>*Key Laboratory of Modern Astronomy and Astrophysics (Nanjing University), Ministry of Education, China*

<sup>3</sup>*School of Physics and Microelectronics, Zhengzhou University, Zhengzhou 450001, China*

<sup>4</sup>*Purple Mountain Observatory, Chinese Academy of Sciences, Nanjing 210023, China*

<sup>5</sup>*Department of Physics, Anhui Normal University, Wuhu, Anhui 241002, China*

<sup>6</sup>*Department of Physics, Nanjing University, Nanjing 210093, China*

We show that it is impossible to experimentally observe the quantum intrinsic orbital angular momentum (IOAM) effect without its axial current. Broadly speaking, we argue that the spiral or interference characteristics of the axial current density determine the occurrence of nonlinear or tunneling effects in any spacetime-dependent quantum systems. Our findings offer a comprehensive theoretical framework that addresses the limitations of Keldysh theory and provides new insights into the angular momentum properties of quantum systems, particularly in tunneling-dominated regimes. Using Wigner function methods, fermionic generalized two-level model, and Berry phase simulations, we predict that IOAM effect can persist even in pure quantum tunneling processes. These results open the door for experimental verification of IOAM effects in future high-intensity QED experiments, such as those using X-ray free electron lasers.

*Introduction.*— The fundamental concepts of the mechanical orbit angular momentum (often referred to extrinsic orbital angular momentum, EOAM) [1], spin angular momentum (SAM) [2] and intrinsic orbital angular momentum (IOAM) [3] play an indispensable role in the study and application of physics. Unlike EOAM, which is defined as  $\mathbf{L} = \mathbf{r} \times \mathbf{P}$ , IOAM describes quantum vortex particles with helical wavefronts characterized by a transverse phase factor  $\exp(i\ell\phi)$  along the propagation direction [4–7]. The IOAM has demonstrated significant potential in various fields, including strong-laser physics, nuclear physics, particle physics, and astrophysics [8–10]. Recent efforts to address the transfer mechanisms of the IOAM have highlighted several critical advancements. These include the generation of vortex  $\gamma$  photons and leptons through spin-to-orbital angular momentum transfer in nonlinear Compton scattering and nonlinear Breit-Wheeler processes [11, 12], the study of helicity transfer mechanisms in the Schwinger effect via multiphoton pair production [13], and the development of quantum manipulation techniques [14, 15], dynamics of relativistic vortex electrons in strong background field [16].

Significant progress has been made in understanding the IOAM through both theoretical and experimental approaches. However, the physical nature, formation mechanisms, and origins of IOAM remain unresolved, making these areas subjects of active research. A key question persists: what physical quantity fundamentally determines formation of the IOAM? While the magnitude of IOAM can be predicted in the multiphoton absorption regime using the Keldysh parameter [17] or effective mass effects [18], significant challenges arise in cases involving tunneling, multi-mechanism processes [19], or dynamically assisted mechanisms [20]. To date, calculating the total IOAM generated within a system or spatial region from a quantum perspective remains a formidable challenge. Additionally, most studies on particles carrying IOAM have primarily focused on multiphoton processes. This raises a crit-

ical question: is it truly impossible to generate vortex particles carrying IOAM through tunneling processes? Moreover, although theoretical studies on the observation and calculation of particle OAM are presented in Ref. [21], it remains unclear whether this OAM belongs to the IOAM or EOAM. Exploring this possibility is an important direction for future research. While Keldysh theory has successfully predicted the occurrence of multiphoton and tunneling processes in purely time- or space-dependent background fields [22–24], its applicability is significantly constrained in non-plane-wave, spacetime-dependent electromagnetic fields [25–27]. Furthermore, no comprehensive theoretical framework currently exists to describe the probability distribution of a particle’s IOAM. In short, the general explanation and physical origins of IOAM remain open and unresolved questions, requiring further exploration.

In this Letter, we show that the IOAM originates from the axial current density. Without the axial current density, there would be no quantum IOAM of particles. The spiral (helical) or interference characteristics of the axial current density determine the occurrence of nonlinear or tunneling effects in the system. This result holds for any spacetime-dependent background field and addresses the shortcomings and limitations of Keldysh theory. By employing the Wigner function method, fermionic generalized two level model, and Berry phase simulations, we have explored potential future experiments on the Schwinger effect. Our findings reveal that the quantum IOAM effect persists even in pure quantum tunneling processes. This may provides new theoretical insights into the angular momentum properties of quantum systems.

*Generalized quantum angular momentum.*— To gain a deeper general understanding and explanation of the physical essence, formation mechanism, and origin of the IOAM, while also revealing the limitations of the existing Keldysh theory and exploring a more universal theoretical framework, we construct a generalized quantum angular momentum based

on the Wigner function [28] to address these issues. The total quantum angular momentum of the quantum system in arbitrarily spacetime-dependent background fields can be written as

$$\mathcal{M} = \overbrace{\int d\Gamma (\mathbf{x} \times \mathbf{p})}_{\text{EOAM of particles}} \mathbb{w}_0 + \overbrace{\int d\Gamma \frac{(-\mathbf{a})}{2}}_{\text{IOAM of particles}} + \overbrace{\int d^3x \mathbf{x} \times (\mathbf{E} \times \mathbf{B})}_{\text{EOAM of gauge field}}, \quad (1)$$

where the first, second, and third terms on the right-hand side of the above equation represent the EOAM of the particles, the IOAM of the particles, and the EOAM of the gauge field, respectively. The phase-space volume is defined as  $d\Gamma = d^3x d^3p / (2\pi\hbar)^3$  [29, 30], in which  $\hbar$  is the reduced Planck constant. Here,  $\mathbb{w}_0$  and  $\mathbf{a}$  denote the charge and axial current densities, respectively [29, 31]. Additionally,  $\mathbf{x}$ ,  $\mathbf{p}$ ,  $\mathbf{E}$  and  $\mathbf{B}$  are the vector position space, momentum, electric field and magnetic field, respectively. If redefine that  $\mathcal{L}_{\text{IOAM}} = -\mathbf{a}/2$  is as intrinsic orbital angular momentum probability density,  $\mathcal{L}_{\text{IOAM}}$  determines the occurrence of nonlinear effects or tunneling effects in any quantum systems. Notably,  $\mathcal{L}_{\text{IOAM}}$  is more fundamental and broader than the Keldsh parameter, it can calculate the total IOAM of the quantum sys-

tem. Without  $\mathcal{L}_{\text{IOAM}}$ , we can not observe any quantum vortex structures in real experiments.

*Generalized spin resolved fermionic quantum two level model.*— To enhance the reliability of our results, we calculated the Berry phase as follows:  $\arg [c_{\mathbf{q}}^{(2)}(t)] = \arctan(\Im [c_{\mathbf{q}}^{(2)}(t)] / \Re [c_{\mathbf{q}}^{(2)}(t)])$ , referencing the foundational work of Berry [32, 33] and  $c_{\mathbf{q}}^{(2)}(t)$  can be obtained from the fermionic generalized two-level model for studying the pair production under any time-dependent electric field in our previous work [34] as

$$c_{\mathbf{q}}^{(2)}(t) = \sum_{\mathbf{s}} \sum_{\mathbf{s}'} c_{\mathbf{q},\mathbf{s},\mathbf{s}'}^{(2)}(t), \quad (2)$$

where

$$i \frac{d}{dt} \begin{bmatrix} c_{\mathbf{q},\mathbf{s},\mathbf{s}'}^{(1)}(t) \\ c_{\mathbf{q},\mathbf{s},\mathbf{s}'}^{(2)}(t) \end{bmatrix} = \begin{pmatrix} \omega_{\mathbf{q}}(t) & i\Omega_{\mathbf{q},\mathbf{s},\mathbf{s}'}(t) \\ -i\Omega_{\mathbf{q},\mathbf{s},\mathbf{s}'}^*(t) & -\omega_{\mathbf{q}}(t) \end{pmatrix} \begin{bmatrix} c_{\mathbf{q},\mathbf{s},\mathbf{s}'}^{(1)}(t) \\ c_{\mathbf{q},\mathbf{s},\mathbf{s}'}^{(2)}(t) \end{bmatrix}, \quad (3)$$

$$\Omega_{\mathbf{q},\mathbf{s},\mathbf{s}'}(t) = \frac{u_{\mathbf{q},\mathbf{s}'}^\dagger(t) \dot{H}_{\mathbf{q}}(t) v_{\mathbf{q},\mathbf{s}}(t)}{2\omega_{\mathbf{q}}(t)}, \quad (4)$$

$$H_{\mathbf{q}}(t) = \begin{pmatrix} m & 0 & p_z(t) & (p_x(t) - ip_y(t)) \\ 0 & m & (p_x(t) + ip_y(t)) & -p_z(t) \\ p_z(t) & (p_x(t) - ip_y(t)) & -m & 0 \\ (p_x(t) + ip_y(t)) & -p_z(t) & 0 & -m \end{pmatrix}, \quad (5)$$

and the initial conditions are  $c_{\mathbf{q},\mathbf{s},\mathbf{s}'}^{(1)}(t_0) = 1$  and  $c_{\mathbf{q},\mathbf{s},\mathbf{s}'}^{(2)}(t_0) = 0$ . One can introduce the kinetic momentum  $\mathbf{p}(t) = \mathbf{q} - e\mathbf{A}(t)$ , where  $\mathbf{q}$  represents the canonical momentum. Here  $\omega_{\mathbf{q}}(t) = \sqrt{m^2 + [\mathbf{q} - e\mathbf{A}(t)]^2}$  is single particle energy. The bispinors are chosen in the following form

$$u_{\mathbf{q},\mathbf{s}} = \sqrt{\frac{(p^0 + m)}{2p^0}} \begin{pmatrix} w_{\mathbf{s}} \\ \frac{\boldsymbol{\sigma} \cdot \mathbf{p}(t)}{(p^0 + m)} w_{\mathbf{s}} \end{pmatrix}, \quad (6)$$

$$v_{\mathbf{q},\mathbf{s}} = \sqrt{\frac{(p^0 + m)}{2p^0}} \begin{pmatrix} \frac{\boldsymbol{\sigma} \cdot \mathbf{p}(t)}{(p^0 + m)} w_{-\mathbf{s}} \\ w_{-\mathbf{s}} \end{pmatrix}, \quad (7)$$

where  $p^0 = p_0 = \sqrt{m^2 + \mathbf{p}^2(t)}$ , and  $w_{+1} = (1, 0)^t$ ,  $w_{-1} = (0, 1)^t$ . The Pauli matrices are

$$\sigma_1 = \begin{pmatrix} 0 & 1 \\ 1 & 0 \end{pmatrix}, \sigma_2 = \begin{pmatrix} 0 & -i \\ i & 0 \end{pmatrix}, \sigma_3 = \begin{pmatrix} 1 & 0 \\ 0 & -1 \end{pmatrix}. \quad (8)$$

The momentum distribution for different spin of electron and positron can be calculated by using the coefficient  $c_{\mathbf{q},\mathbf{s},\mathbf{s}'}^{(2)}$  at  $t = +\infty$  as

$$f_{\mathbf{q}}^{\text{ss}'}(+\infty) = 2|c_{\mathbf{q},\mathbf{s},\mathbf{s}'}^{(2)}(t = +\infty)|^2. \quad (9)$$

The electron and positron momentum distributions are

$$f_{\mathbf{q}}^{\text{s}'}(+\infty) = \sum_{\mathbf{s}} f_{\mathbf{q}}^{\text{ss}'}(+\infty), \quad f_{\mathbf{q}}^{\text{s}}(+\infty) = \sum_{\mathbf{s}'} f_{\mathbf{q}}^{\text{ss}'}(+\infty). \quad (10)$$

The total momentum distribution is

$$f_{\mathbf{q}}(+\infty) = \sum_{\mathbf{s}} \sum_{\mathbf{s}'} f_{\mathbf{q}}^{\text{ss}'}(+\infty). \quad (11)$$

We will then conduct a systematic comparison with the theoretical predictions associated with the  $\mathcal{L}_{\text{IOAM}}$ .

*Setup.*— To validate the aforementioned perspective, we propose conducting theoretical research on potential future experiments related to the Schwinger effect [35–38]. Our idealized experiment involves a representative setup using a circularly polarized (CP) electric field, which is generated by two counter-propagating short laser pulses. Notably, the magnetic fields of the two laser pulses cancel out in the standing wave, resulting in an electric field that is approximately spatially homogeneous throughout the entire interaction region. The electric field can be expressed in a time-dependent form as  $\mathbf{E}(t) = \varepsilon_0 E_{cr} d(t) (\cos(\omega_0 t), \sin(\omega_0 t), 0)$ ,  $d(t) = \sin^4\left(\frac{\omega_0 t}{2N}\right)$  for  $0 < \omega_0 t < 2\pi N$ , where  $\varepsilon_0$  is the peak field strength,  $E_{cr}$  denotes the Schwinger critical field strength,  $\varphi = \omega_0 t$  is the

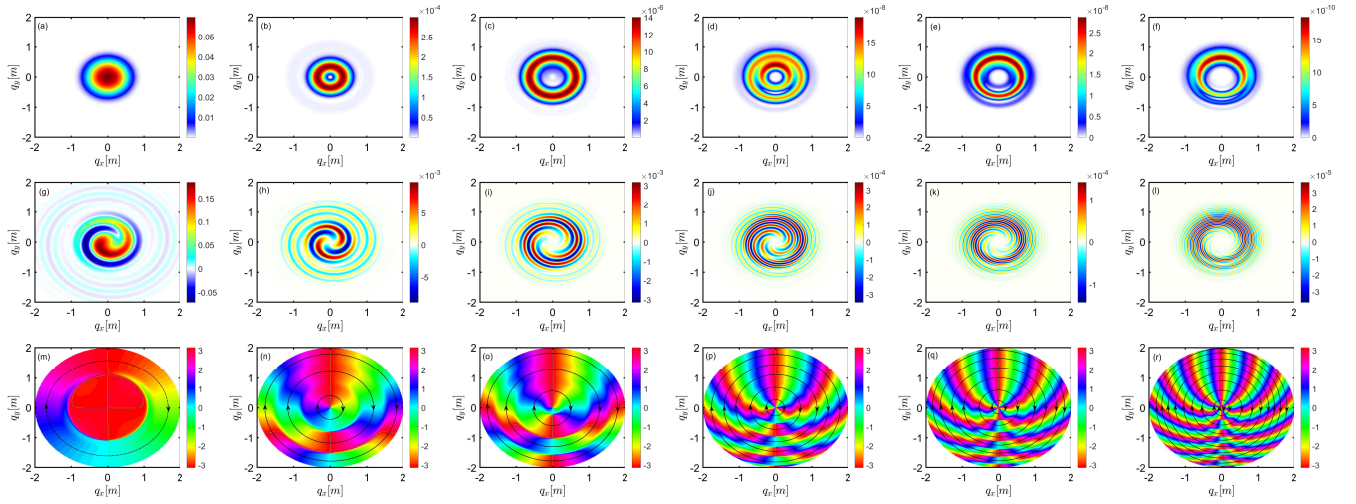


FIG. 1. The first, second, and third rows represent the electron momentum distribution function  $f_{\mathbf{q}}(+\infty)$  (a-f),  $\mathcal{L}_{\text{IOAM}}$  (h-l), and the phase  $\arg[c_{\mathbf{q}}^{(2)}(+\infty)]$  (m-r) for the multiphoton-dominated process, respectively. The first to sixth columns correspond to the absorbed photon numbers of the electron-positron pair, ranging from 1 to 6. The  $\omega_0$  associated with the first to sixth columns are  $2m$ ,  $1m$ ,  $0.8m$ ,  $0.5m$ ,  $0.4m$ , and  $0.3m$ , respectively. For the colorbar associated with  $\mathcal{L}_{\text{IOAM}}$ , positive values indicate that the angular momentum direction is aligned with the  $q_z$  direction, while negative values signify that the angular momentum direction is opposite to the  $q_z$  direction. The other field parameters are  $\varepsilon_0 = 0.1$ ,  $q_z = 0$  and  $N = 6$ .

time-dependent phase of background field,  $\omega_0$  and  $N$  are the frequency and cycle number of the individual electric field, respectively. The pulse duration  $\tau$  is given by  $\tau = 2\pi N/\omega_0 = N\lambda/c$ , where  $\lambda$  is the wavelength and  $c$  is the speed of light. In this latter we use the natural units ( $\hbar = c = 1$ ), and express all quantities in terms of the electron mass  $m$ .

The choice of this scheme is motivated by two primary reasons. First, the particle charge density  $\mathfrak{v}_0$  generated in such a electric field is zero [27]. Second, the absence of a magnetic field eliminates the EOAM contribution from the gauge field. This ensures that IOAM can be investigated precisely without any interference from EOAM effects, see Eq. (1).

*Results.*— Based on the electron momentum distributions shown in Fig. 1 (a-f), we can predict the magnitude and probability distribution of the intrinsic orbital angular momentum  $\mathcal{L}_{\text{IOAM}}$  of electron after the multiphoton process (the Keldysh parameter must satisfy the condition  $\gamma = m\omega_0/\varepsilon\epsilon_0 \gg 1$ ) using the effective mass  $(n\omega_0/2)^2 = q_n^2 + m_*^2$  ( $n$  denotes the absorbed photon number), which theoretically should exhibit concentric circles centered at the origin. However, the observed spiral structures in the intrinsic orbital angular momentum distribution  $\mathcal{L}_{\text{IOAM}}$ , shown as in Fig. 1 (g-l), significantly deviate from the concentric circle pattern. This indicates that simply superimposing the intrinsic angular momentum and its corresponding distribution is not valid. Further analysis reveals that the number of spiral pairs can be estimated using the parameter  $n_s = \lceil \frac{2m}{\omega_0} \rceil$ , in which  $\lceil \cdot \rceil$  is the ceiling function. The corresponding numbers of spiral pairs  $n_s$  in Fig. 1 (a-f) are 1, 2, 3, 4, 5, and 6, respectively. The estimation results are in perfect agreement with the observed spiral structures. Moreover, we observe that the intrinsic orbital angular momentum distribution is entirely confined within the electron

momentum distribution. From Fig. 1 (m-q), we can also extract the possible values of the IOAM of electrons through phase information, given by the relation  $\ell = n_s - s$ , where  $s = 0, 1, 2, \dots, n_s - 1$ . The topological meaning of  $\ell$  can be interpreted as the periodicity or the number of repetitions of color variations starting from the origin. Since the electric field we employ is right-hand circularly polarized, the IOAM exhibits a clockwise rotation direction. This result is consistent with the result in Ref. [13]. The phase information can also explain the origin of nodes in the momentum spectrum. For instance, in Fig.1(m), no vortex effect is observed near the origin, which is why no node forms at the origin in the electron momentum spectrum shown in Fig.1(a). Similarly, in Fig.1(n-r), the presence of vortex effects at the origin leads to distinct nodes at the origin in the electron momentum spectra of Fig.1(b-f).

Next, by comparing the results of multiphoton dominated, multimechanism dominated ( $\gamma = m\omega_0/\varepsilon\epsilon_0 \sim 1$ ), and tunneling dominated ( $\gamma = m\omega_0/\varepsilon\epsilon_0 \ll 1$ ) processes, we thoroughly discuss the validity and physical implications of the IOAM, as shown as Fig. 2 (a-i). Overall, in the multiphoton-dominated regime, the electron momentum distribution,  $\mathcal{L}_{\text{IOAM}}$ , and phase  $\arg[c_{\mathbf{q}}^{(2)}(+\infty)]$  exhibit clear features, as shown in Fig. 2 (a, d, g), requiring no further explanation. However, in the multimechanism-dominated regime, see Fig. 2. (b, e, h), both the  $\mathcal{L}_{\text{IOAM}}$  and  $\arg[c_{\mathbf{q}}^{(2)}(+\infty)]$  display pronounced spiral structures and interference effects. Notably, the phase information can not accurately estimate the specific values of IOAM, indicating that the effective mass model is insufficient for precisely determining IOAM characteristics. Nevertheless, the  $\mathcal{L}_{\text{IOAM}}$  still provides information about the total IOAM. In the tunneling-dominated regime, see Fig. 2. (c, f, i),



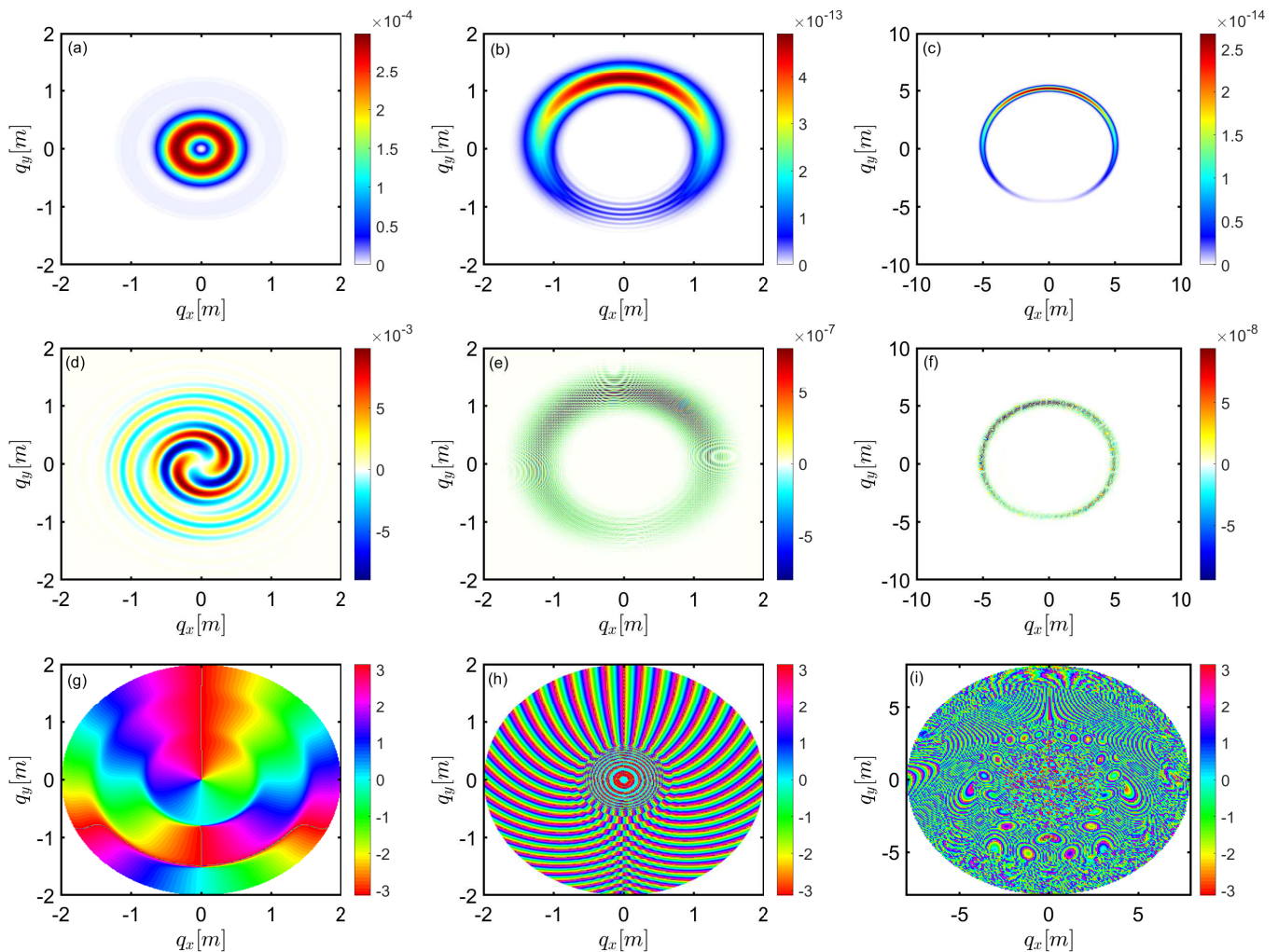


FIG. 2. The first, second, and third rows correspond to the electron momentum distribution function  $f_{\mathbf{q}}(+\infty)$  (a-c),  $\mathcal{L}_{\text{IOAM}}$  (d-f), and the phase  $\arg[c_{\mathbf{q}}^{(2)}(+\infty)]$  (g-i), respectively. The first, second, and third columns represent the multiphoton-dominated process, the multimechanism-dominated process (where both multiphoton and tunneling regimes coexist), and the tunneling-dominated process, respectively. The  $\omega_0$  are set to  $1m$ ,  $0.1m$ , and  $0.02m$  for the multiphoton-dominated, multimechanism-dominated, and tunneling-dominated processes, respectively. For the colorbar associated with  $\mathcal{L}_{\text{IOAM}}$ , positive values indicate that the angular momentum direction is aligned with the  $q_z$  direction, while negative values signify that the angular momentum direction is opposite to the  $q_z$  direction. Other field parameters are  $\varepsilon_0 = 0.1$ ,  $q_z = 0$  and  $N = 6$ .

the  $\mathcal{L}_{\text{IOAM}}$  remains non-zero but manifests solely as pure interference effects. Simultaneously, the phase  $\arg[c_{\mathbf{q}}^{(2)}(+\infty)]$  exhibits irregular interference patterns, suggesting that the phase information becomes entirely ineffective in the tunneling process. However, according to current theoretical understanding, such phenomena are considered impossible. From a theoretical perspective, the already operational X-ray free electron laser (XFEL) facilities, such as the Linac Coherent Light Source (LCLS) at SLAC and TESLA at DESY, can in principle achieve near-critical field strengths as large as  $E \approx 0.1E_{cr}$ , with corresponding laser frequencies of about  $\omega_0 = 8.3 \text{ keV} \approx 0.02m$  [35], corresponding simulation results are shown in Fig. 2. (c, f, i). This result suggests that in future pure tunneling experiments, we may observe the IOAM effect.

*Conclusions.*— In this work, we demonstrated that the in-

trinsic orbital angular momentum (IOAM) originates from axial current density. Without axial current density, the quantum IOAM of particles cannot exist. The spiral or interference characteristics of axial current density are shown to determine the occurrence of nonlinear or tunneling effects within the system. This result is valid for any spacetime-dependent background field, addressing the limitations of the Keldysh theory and providing a more comprehensive theoretical framework.

Using Wigner function methods, a fermionic generalized two-level model, and Berry phase simulations, we predicted that IOAM effects can persist even in pure quantum tunneling processes. Notably, our findings suggest that it is possible to observe IOAM effects experimentally in future tunneling-dominated regimes, as supported by simulations related to operational XFEL facilities like LCLS and TESLA. These findings open new avenues for exploring strong-field quan-

tum electrodynamics (QED) phenomena and offer valuable insights into the angular momentum properties of quantum systems.

*Acknowledgments.*— This work was supported by the National Natural Science Foundation of China (NSFC) under Grant Nos. 12447179, 12233002, 12005192, 12273113. YFH was also supported by National SKA Program of China No. 2020SKA0120300, by the National Key R&D Program of China (2021YFA0718500), and by the Xinjiang Tianchi Program. Cheng-Ming Li was also supported by the Natural Science Foundation of Henan Province of China (No. 242300421375) and by the Project funded by China Postdoctoral Science Foundation (Grant Nos. 2020TQ0287 and 2020M672255). Jin-Jun Geng acknowledges support from the Youth Innovation Promotion Association (2023331).

\* Correspondence Author. email: orkashamat@nju.edu.cn

† Correspondence Author. email: hyf@nju.edu.cn

- [1] I. Newton, *Philosophiæ Naturalis Principia Mathematica* (Royal Society, London, 1687).
- [2] G. E. Uhlenbeck and S. Goudsmit, Spinning Electrons and the Structure of Spectra, *Nature* **117**, 264 (1926).
- [3] L. Allen, M. W. Beijersbergen, R. J. C. Spreeuw, and J. P. Woerdman, Orbital angular momentum of light and the transformation of Laguerre-Gaussian laser modes, *Phys. Rev. A* **45**, 8185 (1992).
- [4] U. D. Jentschura and V. G. Serbo, Generation of High-Energy Photons with Large Orbital Angular Momentum by Compton Backscattering, *Phys. Rev. Lett.* **106**, 013001 (2011).
- [5] K. Y. Bliokh, M. R. Dennis, and F. Nori Relativistic Electron Vortex Beams: Angular Momentum and Spin-Orbit Interaction, *Phys. Rev. Lett.* **107**, 174802 (2011).
- [6] K. Y. Bliokh, F. J. Rodríguez-Fortuño, F. Nori, and A. V. Zayats, Spin-orbit interactions of light, *Nature Photon.* **9**, 796 (2015).
- [7] M. J. Padgett, Orbital angular momentum 25 years on [invited], *Opt. Express* **25**, 11265 (2017).
- [8] K. Y. Bliokh, I. P. Ivanov, G. Guzzinati, L. Clark, R. Van Boxem, A. Béché, R. Juchtmans, M. A. Alonso, P. Schattschneider, and F. Nori, *et al.* Theory and applications of free-electron vortex states, *Phys. Rept.* **690**, 1 (2017).
- [9] I. P. Ivanov, Promises and challenges of high-energy vortex states collisions, *Prog. Part. Nucl. Phys.* **127**, 103987 (2022).
- [10] D. Session, M. J. Mehrabad, N. Paithankar, T. Grass, C. J. Eckhardt, B. Cao, D. G. S. Forero, K. Li, M. S. Alam, and K. Watanabe, *et al.* Optical pumping of electronic quantum Hall states with vortex light, *Nature Photon.* (2024).
- [11] M. Ababekri, R. T. Guo, F. Wan, B. Qiao, Z. Li, C. Lv, B. Zhang, W. Zhou, Y. Gu, and J. X. Li, Vortex  $\gamma$  photon generation via spin-to-orbital angular momentum transfer in nonlinear Compton scattering, *Phys. Rev. D* **109**, 016005 (2024).
- [12] M. Ababekri, J. L. Zhou, R. T. Guo, Y. Z. Ren, Y. H. Kou, Q. Zhao, Z. P. Li, and J. X. Li, Generation of ultrarelativistic vortex leptons with large orbital angular momenta, *Phys. Rev. D* **110**, 076024 (2024).
- [13] C. Kohlfürst, Pair production in circularly polarized waves, *Phys. Rev. D* **110**, L111903 (2024).
- [14] Z. W. Lu, L. Guo, Z. Z. Li, M. Ababekri, F. Q. Chen, C. Fu, C. Lv, R. Xu, X. Kong and Y. F. Niu, *et al.* Manipulation of Giant Multipole Resonances via Vortex  $\gamma$  Photons, *Phys. Rev. Lett.* **131**, 202502 (2023).
- [15] J. J. Jiang, K. H. Zhuang, J. D. Chen, J. X. Li, and Y. Y. Chen, Manipulation of spin and orbital angular momenta of  $\gamma$  photon in nonlinear Compton scattering, [arXiv:2410.20658 [hep-ph]].
- [16] M. Ababekri, Y. Wang, R. T. Guo, Z. P. Li, and J. X. Li, Dynamics of relativistic vortex electrons in external laser fields, *Phys. Rev. A* **110**, 052207 (2024).
- [17] L. V. Keldysh, Ionization in the Field of a Strong Electromagnetic Wave, *J. Exp. Theor. Phys.* **20**, 1307 (1965).
- [18] C. Kohlfürst, H. Gies, and R. Alkofer, Effective mass signatures in multiphoton pair production, *Phys. Rev. Lett.* **112**, 050402 (2014).
- [19] C. Kohlfürst, Effect of time-dependent inhomogeneous magnetic fields on the particle momentum spectrum in electron-positron pair production, *Phys. Rev. D* **101**, 096003 (2020).
- [20] R. Schutzhold, H. Gies, and G. Dunne, Dynamically assisted Schwinger mechanism, *Phys. Rev. Lett.* **101**, 130404 (2008).
- [21] X. D. Ji, Gauge-Invariant Decomposition of Nucleon Spin, *Phys. Rev. Lett.* **78**, 610 (1997).
- [22] G. V. Dunne and C. Schubert, Worldline instantons and pair production in inhomogeneous fields, *Phys. Rev. D* **72**, 105004 (2005).
- [23] G. V. Dunne, Q. h. Wang, H. Gies, and C. Schubert, Worldline instantons. II. The Fluctuation prefactor, *Phys. Rev. D* **73**, 065028 (2006).
- [24] O. Amat, L. N. Hu, A. Sawut, M. Mohamedsedik, M. A. Bake, and B. S. Xie, Schwinger pair production rate and time for some space-dependent fields via worldline instantons formalism, *Eur. Phys. J. D* **76**, 188 (2022).
- [25] C. Schneider and R. Schützhold, Dynamically assisted Sauter-Schwinger effect in inhomogeneous electric fields, *JHEP* **02**, 164 (2016).
- [26] C. Schneider, G. Torgrimsson, and R. Schützhold, Discrete worldline instantons, *Phys. Rev. D* **98**, 085009 (2018).
- [27] O. Amat, L. N. Hu, M. A. Bake, M. Mohamedsedik, and B. S. Xie, Effect of spatially oscillating field on Schwinger pair production, *Phys. Rev. D* **108**, 056011 (2023).
- [28] M. E. Peskin, *An Introduction to Quantum Field Theory* (CRC Press, Boca Raton, 2018).
- [29] I. Bialynicki-Birula, P. Gornicki, and J. Rafelski, Phase space structure of the Dirac vacuum, *Phys. Rev. D* **44**, 1825 (1991).
- [30] F. Hebenstreit, Ph.D. thesis, Schwinger effect in inhomogeneous electric fields, [arXiv:1106.5965 [hep-ph]].
- [31] X. L. Sheng, Ph.D. thesis, Wigner Function for Spin-1/2 Fermions in Electromagnetic Fields, [arXiv:1912.01169 [hep-ph]].
- [32] M. V. Berry, Quantal phase factors accompanying adiabatic changes, *Proc. Roy. Soc. Lond. A* **392**, 45 (1984).
- [33] Bialynicki-Birula, Iwo and Bialynicka-Birula, Zofia, and Śliwa, Cezary, Motion of vortex lines in quantum mechanics, *Phys. Rev. A* **61**, 032110 (2000).
- [34] O. Amat, H. H. Fan, S. Tang, Y. F. Huang, and B. S. Xie, Spin resolved momentum spectra for vacuum pair production via a generalized two level model, [arXiv:2409.11833 [hep-ph]].
- [35] A. Ringwald, Pair production from vacuum at the focus of an X-ray free electron laser, *Phys. Lett. B* **510**, 107 (2001).
- [36] R. Alkofer, M. B. Hecht, C. D. Roberts, S. M. Schmidt, and D. V. Vinnik, Pair creation and an x-ray free electron laser, *Phys. Rev. Lett.* **87**, 193902 (2001).
- [37] T. Heinzl and A. Ilderton, Exploring high-intensity QED at ELI, *Eur. Phys. J. D* **55**, 359 (2009).
- [38] A. Fedotov, A. Ilderton, F. Karbstein, B. King, D. Seipt, H. Taya, and G. Torgrimsson, Advances in QED with intense

